U.S. DEPARTMENT OF ENERGY

PNNL- 20689

Prepared for the U.S. Department of Energy
under Contract DE-AC05-76RL01830

Lead Slowing-Down Spectrometry for Spent Fuel Assay: FY11 Status Report

G Warren, K Anderson, B Becker[2], D. Beller[4], SM Bowyer
AM Casella, Y Danon[2], M Devlin[1], A Gavron[1], C. Gesh
RC Haight[1], D Hatchett[4], G Imel[3], J Kulisek, JM O'Donnell[1]

August 2011

[1] Los Alamos National Laboratory, Los Alamos, NM 87545
[2] Rensselaer Polytechnic Institute, Troy, NY 12180
[3] Idaho State University, Pocatello, ID 83204
[4] University of Nevada, Las Vegas, Las Vegas, NV 89054

Pacific Northwest
NATIONAL LABORATORY

DISCLAIMER

PACIFIC NORTHWEST NATIONAL LABORATORY
operated by
BATTELLE
for the
UNITED STATES DEPARTMENT OF ENERGY
under Contract DE-AC05-76RL01830

Printed in the United States of America

Available to DOE and DOE contractors from the
Office of Scientific and Technical Information,
P.O. Box 62, Oak Ridge, TN 37831-0062;
ph: (865) 576-8401
fax: (865) 576-5728
email: reports@adonis.osti.gov

Available to the public from the National Technical Information Service,
U.S. Department of Commerce, 5285 Port Royal Rd., Springfield, VA 22161
ph: (800) 553-6847
fax: (703) 605-6900
email: orders@ntis.fedworld.gov
online ordering: http://www.ntis.gov/ordering.htm

This document was printed on recycled paper.
(9/2003)

PNNL-20689

Lead Slowing-Down Spectrometry for Spent Fuel Assay: FY11 Status Report

G Warren, K Anderson, B Becker[2], D. Beller[4]
SM Bowyer, AM Casella, Y Danon[2], M Devlin[1]
A Gavron[1], C Gesh, RC Haight[1], D Hatchett[4]
G Imel[3], J Kulisek, JM O'Donnell[1]

August 2011

Prepared *for the* U. S. DEPARTMENT OF ENERGY
under Contract DE-AC05-76RL01830

Pacific Northwest National Laboratory
Richland, WA 99354

---

[1] Los Alamos National Laboratory, Los Alamos, NM 87545
[2] Rensselaer Polytechnic Institute, Troy, NY 12180
[3] Idaho State University, Pocatello, ID 83204
[4] University of Nevada, Las Vegas, Las Vegas, NV 89054

Acknowledgments

The authors would like to thank all the project collaborators including:

Mark Shaver (PNNL) and Eric Smith (currently at the International Atomic Energy Agency).

We would also like to acknowledge the Department of Energy Fuel Cycle Research and Development Program, Material Protection, Accounting, and Control Technology (MPACT) Campaign for their support in funding this work.

Executive Summary

Developing a method for the accurate, direct, and independent assay of the fissile isotopes in bulk materials (such as used fuel) from next-generation domestic nuclear fuel cycles is a goal of the Office of Nuclear Energy, Fuel Cycle R&D, Material Protection and Control Technology (MPACT) Campaign. To meet this goal, MPACT supports a multi-institutional collaboration to study the feasibility of Lead Slowing Down Spectroscopy (LSDS). This technique is an active nondestructive assay method that has the potential to provide independent, direct measurement of Pu and U isotopic masses in used fuel with an uncertainty considerably lower than the approximately 10% typical of today's confirmatory assay methods. This document is a progress report for FY2011 collaboration activities.

Progress made by the collaboration in FY2011 continues to indicate the promise of LSDS techniques applied to used fuel. PNNL developed an empirical model based on calibration of the LSDS to responses generated from well-characterized used fuel. The empirical model demonstrated the potential for the direct and independent assay of the sum of the masses of ^{239}Pu and ^{241}Pu to within approximately 3% over a wide used fuel parameter space. Similar results were obtained using a perturbation approach developed by LANL. Benchmark measurements have been successfully conducted at LANL and at RPI using their respective LSDS instruments. The ISU and UNLV collaborative effort is focused on the fabrication and testing of prototype fission chambers lined with ultra-depleted ^{238}U and ^{232}Th, and uranium deposition on a stainless steel disc.

In FY2012, the collaboration plans a broad array of activities. PNNL will focus on optimizing its empirical model and minimizing its reliance on calibration data, as well as continuing efforts towards developing an analytical model. Additional measurements are planned at LANL and RPI. LANL measurements will include a Pu sample, which is expected to provide more counts at longer slowing-down times to help identify discrepancies between experimental data and MCNPX simulations. RPI measurements will include the assay of an entire fresh fuel assembly for the study of self-shielding effects as well as the ability to detect diversion by detecting a missing fuel pin in the fuel assembly. The development of threshold neutron sensors will continue, and UNLV will calibrate existing ultra-depleted uranium deposits at ISU.

Symbols, Acronyms and/or Initialisms

BTB FC's	Back-to-Back Fission Chambers
ENDF	Evaluated Nuclear Data File
FWHM	Full-width at half max
GWd/MTU	Gigawatt days per metric ton of uranium
IAEA	International Atomic Energy Agency
ISU	Idaho State University
LANL	Los Alamos National Laboratory
LSDS	Lead Slowing-down Spectroscopy
NDA	Non-destructive assay
PNNL	Pacific Northwest National Laboratory
PWR	Pressurized water reactor
RPI	Rensselaer Polytechnic Institute
RTIL	Room temperature ionic liquid
SNL	Sandia National Laboratories
SS	Stainless steel
uDU	Ultra-depleted uranium
UNLV	University of Nevada Las Vegas
VR	Variance reduction
ε	percent error: 100×|true-estimate|/true

Contents

Figures

1.0 Introduction

Nondestructive assay (NDA) for quantifying the amount of the individual Pu isotopes (i.e. ^{239}Pu, ^{240}Pu, ^{241}Pu) in used fuel assemblies is important for nuclear safeguards and used fuel storage. With respect to nuclear safeguards, it is necessary for determining shipper-receiver difference and retaining or recovering continuity of knowledge. Also, such measurements can be used to support criticality calculations by verifying fuel burnup in order to maximize used fuel capacity in short-term and long-term fuel storage, and to optimize the efficient transport of used fuel.

Current NDA methods infer total Pu mass using a combination of burnup codes for calculating isotopic inventories and passive measurements of easily measured isotopes in used fuel (e.g. ^{137}Cs and ^{244}Cm). The International Atomic Energy Agency (IAEA) has determined that such methods typically carry a Pu uncertainty of approximately 10% [1], which may result in an unaccounted Pu mass of more than 1000 kg per year in a high-volume storage or reprocessing facility.

To address these issues, this work focuses on the application of the lead slowing down spectrometer (LSDS), a well-established active interrogation technique having a long and extensive history for use in nuclear cross-section measurements [2,3], to the measurement of isotopic masses in used fuel. The goal of this effort is to use the LSDS to directly measure fissile isotopes (e.g. ^{235}U, ^{239}Pu, and ^{241}Pu) in used fuel assemblies with significantly better accuracy, with minimal externally provided (operator-declared) information, and in a time-efficient manner. An example of an appropriate place for the LSDS in a fuel cycle would be at the receiving end of a reprocessing facility.

Previous studies, predominantly simulation-based, highlighted the potential of the LSDS method to directly measure both Pu and U isotopes in used fuel but often made optimistic assumptions about pulsed-neutron source intensity, the availability and efficacy of threshold neutron detection technologies, and the impact of potentially degrading background source terms. Realizing the potential of LSDS, therefore, depends on addressing those assumptions and the resulting technical challenges. Under funding from the Department of Energy Office of Nuclear Energy's Material Protection, Accounting, and Control Technology (MPACT) program, a collaboration was formed to study these technical challenges and advance the understanding of LSDS for fuel assay. The collaboration consists of Pacific Northwest National Laboratory (PNNL), Los Alamos National Laboratory (LANL), Rensselaer Polytechnic Institute (RPI), Idaho State University (ISU) and the University of Nevada-Las Vegas (UNLV). This paper begins with a brief overview of the principles of LSDS for fuel assay then describes recent progress in addressing the technical challenges described above.

Developments to date include the following:

1. *Development of a detailed model that can be simulated with standard neutron transport codes such as MCNP/MCNPX [4]*

   Models have been developed by PNNL in collaboration with LANL, and similar modeling has been performed at RPI. They have been used extensively for evaluating the response of an LSDS system to different types of used fuel, evaluating analysis models, and calculating rates in detectors.

2. *Benchmarking the simulations against experimental data at existing LSDS systems*

   Benchmarking simulations in comparison to experimental data has taken place at LANL and RPI. Benchmarking at LANL included the effects of the reflection of neutrons from the surrounding environment, and the effect of small (but non-negligible) impurities, on the scale of parts-per-million, in the lead. In general, very good agreement has been obtained between the simulations and experimental data, except for the energy region below 10 eV where nuclear data for lead scattering may need improvement. RPI has conducted experiments with its LSDS, assaying a fresh fuel pin containing 32.5 g of ^{235}U both separately and in conjunction with a PuBe source containing 96 grams of ^{239}Pu. In addition, RPI has recently assayed a fresh fuel pin combined with additional small discs each consisting of 0.2 g of ^{235}U in order to assess the sensitivity of the LSDS for ^{235}U assay.

3. *Developing tools to analyze the time-spectra produced by the LSDS*

   PNNL and LANL have independently developed tools to calculate the quantities of fissile materials in the used fuel. PNNL continued to study and refine the analytical model. While the understanding of the analytical model was improved, there was little improvement in the uncertainties of the extracted isotopic masses. As an alternative to the analytical model, PNNL developed an empirical model involving calibration of the LSDS to responses generated from well-characterized assemblies and continued efforts in developing an analytical model to account for self-shielding. The empirical approach shows the promise of significantly reducing the uncertainties of the extracted isotopic masses to below 3%. LANL essentially used a perturbation approach – a precise calculation was performed with MCNPX, and small deviations from the concentrations used a simplistic model to determine the required correction.

4. *Developing neutron detector systems that discriminate against the slow neutrons*

   A critical component of the LSDS is the detection of the fast fission neutrons, which are distinct from the slower interrogating neutrons that need to be discrimanted against. The ISU and UNLV collaborative effort is focused on the fabrication and testing of prototype fission chambers lined with ultra-depleted ^{238}U and ^{232}Th, which

are threshold-fissioning isotopes. UNLV has been successful at U deposition on a stainless steel disc (SS) using spiked U_3O_8 from Room Temperature Ionic Liquid (RTIL). There are concerns about the availability of appropriate quantities of ultra-depleted ^{238}U (100's of grams per LSDS), which may force the emphasis to ^{232}Th if the detector technology is to remain fission chambers. Unfortunately, ^{232}Th has one-quarter of the cross section of ^{238}U, which would lead to lower efficiency, and hence, lower count rate. A new suggestion involves the use of helium pressurized tubes, where the helium recoil from the scattering of a neutron is registered. Very preliminary calculations show that this may be a viable alternative.

2.0 Principles of LSDS for Fuel Assay

The use of the LSDS for the NDA of used fuel assemblies is based on the unique resonance structure of the cross sections of each of the isotopes in the fuel, which are strong functions of the incident neutron energy. The incident neutron energy, *E*, is, in turn, determined in the LSDS as a function of time, *t*, from the initiation of a neutron beam pulse. A simplified schematic of an LSDS is shown in Figure 2-1. In the LSDS, the interrogating neutrons, initially having several MeV of energy from a pulsed neutron source (e.g. LINAC), are injected into the Pb of the LSDS. Within approximately a microsecond, they slow down and lose energy via inelastic collisions with the Pb nuclei such that the mean interrogating neutron energy decreases to approximately 100 keV. At that time (and neutron energy), elastic scattering becomes the dominate interaction method. Then the relationship between *E* and *t* in the Pb is given by (1), and the energy resolution, which is roughly independent of time, is given by (2) [5].

$$E = \frac{k}{(t + t_0)^2}, \tag{1}$$

$$\frac{\Delta E}{E} = \sqrt{\frac{8}{3A}}. \tag{2}$$

The underlying assumption of (1) and (2) is that the Pb is completely free from impurities, particularly those having light atomic mass, such as hydrogen. Consequently, the fuel must be completely dry before being placed in the LSDS. The presence of the fuel assembly in the LSDS interrogation chamber also has an appreciable effect on (1) and (2) [6].

As the interrogating neutrons slow down in the Pb, they induce fissions of the various isotopes in the fissile sample. The prompt fission neutrons emitted by these fissile isotopes in the sample contribute to the signal generated in the assay-signal sensors (e.g. fission chambers containing ^{232}Th or ^{238}U). The fission neutrons can be distinguished from the interrogating neutrons by their energy. As ^{232}Th and ^{238}U have very low fission cross sections at low energies (< 100 μb), they make ideal materials for assay chambers to detect the fast fission neutrons.

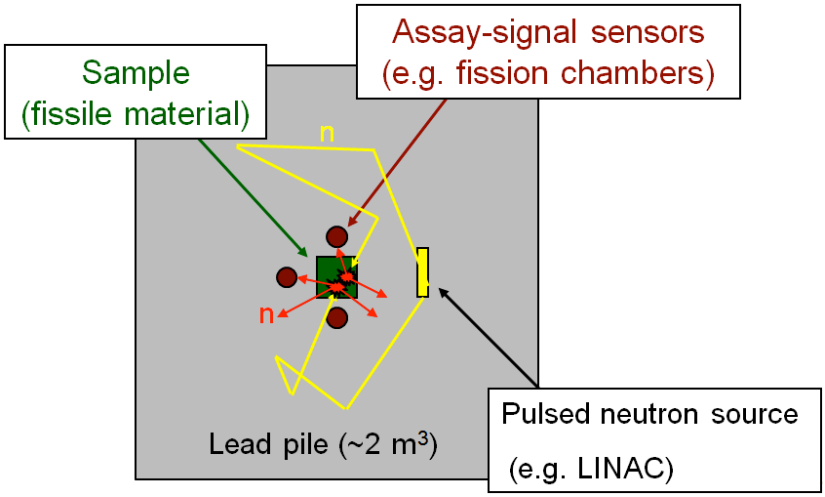

Figure 2-1. Simplified schematic of an LSDS illustrating components and operation.

3.0 Time-Spectral Analysis Methods

3.1 PNNL Methods

A schematic of the PNNL design of an LSDS for use in the NDA of used nuclear fuel is shown in Figure 3-1**Error! Reference source not found.**. This figure also illustrates the process for determining the isotopic masses in the fuel assembly. As the interrogating neutrons slow down in the Pb, they induce fissions of various isotopes in the fuel at a rate proportional to the integral of the energy-dependent neutron flux multiplied by the fissile cross sections of the isotopes in the fuel. Additionally, the interrogating neutrons induce fissions in the isotopic fission chambers, which are each comprised of one of the isotopes of interest (e.g. ^{235}U and ^{239}Pu) assumed to be present in the fuel assembly. The individual signals, $x_i(t)$, from each of the isotopic fission chambers then serve as empirical basis vectors to deconvolve the assay signal, $y(t)$, from the threshold fission chambers (lined with either ^{238}U or ^{232}Th), which serve to detect the prompt fission neutrons emitted from the fuel. Examples of simulated isotope response functions and assay signals are shown in Figure 3-2**Error! Reference source not found.**.

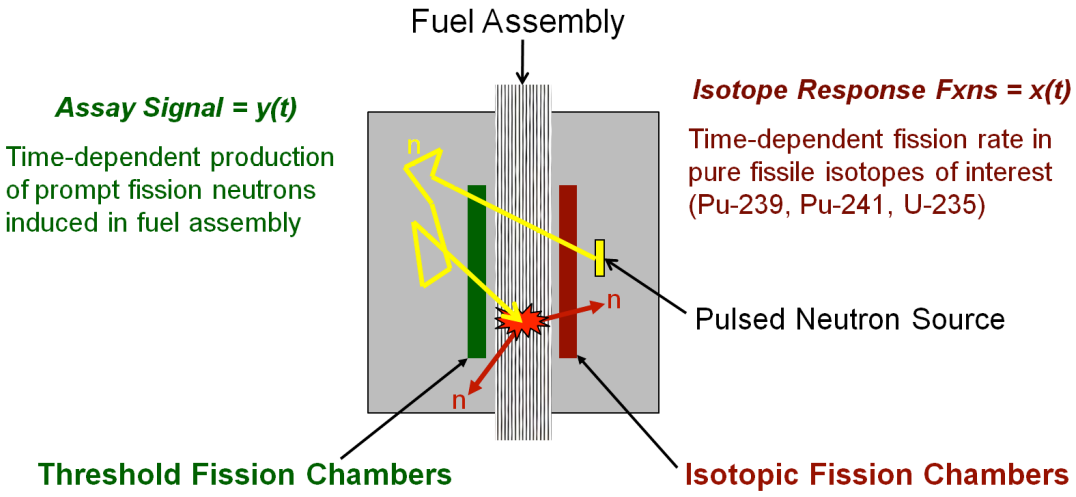

Figure 3-1. Schematic of the PNNL model of a lead slowing-down spectrometer for fuel assay. The interrogating neutron population induces fission in the fuel assembly and isotopic fission chambers, and threshold fission chambers record the time-dependent production of prompt fission neutrons [6].

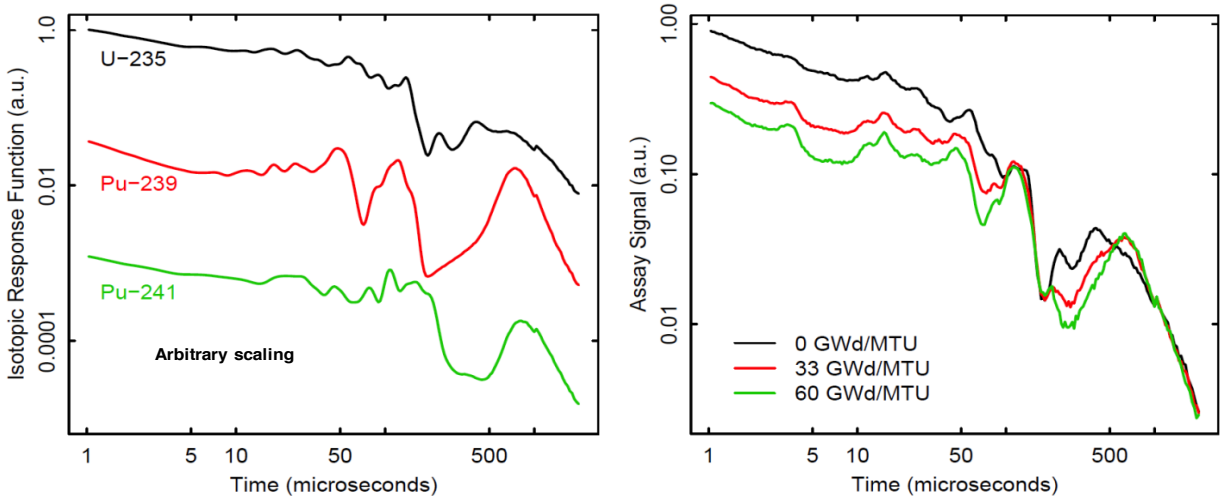

Figure 3-2. Example LSDS time spectra from the PNNL LSDS design: Isotope response functions, *x(t)*, for the three primary fissile isotopes of interest (left), and simulated assay signals, *y(t)*, from PWR fuels of various burnup levels (right) [6].

Currently, no LSDS that can assay full, used fuel assemblies is available to evaluate the LSDS methods described here. Therefore, this work currently relies on the fuel assembly library developed by LANL [7], which consists of 64 used fuel assemblies ranging in initial ^{235}U loading from 2% to 5%, 15 to 60 GWd/MTU burnup, 1 to 80 years cooling time, and 10 ppm per 1 GWd/MTU of hydrogen concentration in the fuel cladding. Also, variation in radial burnup

within each fuel pin, as well as variation in burnup among each separate fuel pin exists within each of the 64 fuel assembly models. In MCNPX, the fuel assembly models were placed inside the assay chamber of a nominal LSDS instrument [6] to simulate the assay and to evaluate the mathematical models used to extract the masses of the isotopes.

The assay signal y(t) is expected to be a linear combination of the isotopic response functions, $x_i(t)$:

$$y(t) = C\left[a_{235}x_{235}(t) + a_{239}x_{239}(t) + a_{241}x_{241}(t)\right] = C\sum_i a_i x_i(t), \tag{3}$$

where 235 indicates ^{235}U, 239 indicates ^{239}Pu and 241 indicates ^{241}Pu. In (3), it is assumed for simplicity, that the efficiencies of each of the isotopic fission chambers used in the PNNL design are the same. The isotopic coefficients, a_i, are proportional to the corresponding isotopic masses, m_i, in the fuel.

One must account for the self-shielding effect caused by the presence of strong absorbers in the fuel assembly. This effect alters the interrogating neutron flux such that flux in the fuel, $\phi_{fuel}(t)$, is not equal to the flux in the fission chambers, $\phi_{detectors}(t)$. In order to account for the self-shielding, a time-dependent self-shielding function, $f(t)$, is introduced:

$$y(t) = f(t)C\sum_i \frac{m_i \nu_i}{A_i} x_i(t), \tag{4}$$

where ν_i is the average number of neutrons released per fission and A_i is the atomic weight of the isotope. Equation (4) assumes for simplicity that in addition to the assumptions upon which (3) is based, each isotopic fission chamber contains the same number of fissile nuclei.

The self-shielding function, $f(t)$, is defined as:

$$f(t) = \frac{\bar{\phi}_{fuel}(t)}{\phi_{detectors}(t)}. \tag{5}$$

Thus in this scheme applied by PNNL, in order to extract the isotopic masses m_i, it is necessary to measure the assay signal $y(t)$ and the isotopic responses $x_i(t)$ as well as have a means to determine the self-shielding function $f(t)$.

3.1.1 PNNL Analytical Approach for Approximating Self-Shielding

In FY2010, PNNL developed a first-generation analytical $f(t)$ that accounts for self-shielding so that the masses of fissile ^{235}U, ^{239}Pu, ^{240}Pu and ^{241}Pu can be determined as well as the masses of non-fissile isotopes that cause significant absorption. It is important to note that in this first-generation formulation, the fuel is considered as a simple, homogeneous, right parallelepiped of length H and edge dimension L. Further, it is assumed that the reaction cross-sections can be expressed in terms of slowing time, using the slowing-time versus energy relationship in Eq. 1. This formulation for the self-shielding function is:

$$f(t) = \frac{1 - e^{-\left(\frac{2N_A}{L(L+2H)}\sum_i \frac{m_i}{A_i}(\sigma_f(t)+\sigma_c(t))_i\right)}}{\frac{2N_A}{L(L+2H)}\sum_i \frac{m_i}{A_i}(\sigma_f(t)+\sigma_c(t))_i} \tag{6}$$

where N_A is Avogadro's number, H and L are the fuel dimensions as described above, and σ_f and σ_c are the microscopic fission and capture cross-sections for isotope i as a function of slowing-down time [8].

In FY2011, initial work at PNNL was focused on verifying and improving the implementation of $f(t)$ as formulated in (6):

- The impact of extending the selection of isotopes included in (6) was studied. Accounting for the top 20 absorbers in the self-shielding function provided little improvement compared to the original top 5 absorbers.
- It was discovered that absorption and scattering in the ^{238}U dominates the deviation of the flux in the fuel from the incident neutron flux that is generating the $x(t)$ signals in the isotopic fission chambers.
- The TallyX feature of MCNPX was used to calculate the actual mean chord length of the neutron paths through the assembly. This value replaced the original Dirac mean chord length in the analytical model, which was based on the assumption of isotropic and uniform flux.
- The inequality of the flux in the fission chambers compared to the flux in the empty assay chamber (case with no fuel assembly) was taken into account in the model.

Although these modifications generally improved the agreement between the analytical $f(t)$ and the $f(t)$ obtained by dividing the actual average flux in the fuel by the actual average flux in the surrounding detectors as tallied in the MCNP simulations [8], no significant improvement in the accuracy of the calculated mass estimates resulted. Thus, the first-generation $f(t)$ would need to be significantly modified.

A new formulation of the self-shielding function would need to account for major deficiencies. For instance, results from MCNPX simulations conducted in FY2011 indicated that the presence

of the fuel assembly in the LSDS caused a significant depression of the interrogation neutron flux in the fission chambers surrounding the fuel assembly. In addition, it is likely that the neglect of scattering within the fuel assembly and the neglect of streaming of incident neutrons between the fuel pins within the fuel lattice may also contribute discrepancies between the analytical $f(t)$ and the $f(t)$ determined directly from the MCNPX simulations.

3.1.2 PNNL Empirical Approach for Approximating Self-Shielding

As an alternative to the above analytical approach, an empirical model was developed to verify that the *y(t)* and *x(t)* signals generated within the LSDS were sufficiently accurate to distinguish between the various assemblies within the standard NGSI 64 library. This approach was based on calibration and a numerical approximation to $f(t)$ using singular value decomposition (SVD) [9]. The SVD technique reduced the data to a set of empirical basis vectors to approximate $f(t)$'s for each of the 64 LANL fuels. This technique avoided the rigidity imposed by the analytical model, which was based on assumptions determined to be inaccurate for a one-meter long portion of an entire fuel assembly [8].

For this algorithm, the 64 true $f(t)$'s were determined. For each of the 64 used fuel assembly models in the LANL 64, the true m_i's from the MCNP input decks were inserted into (4), which was then used to solve for $f(t)$. The $f(t)$'s spanned 162 time bins ranging from 20 μs to 2000 μs. A value of 1.0 was subtracted from each of these $f(t)$'s to improve the numerical stability when performing the final step of determining the unknown masses using a nonlinear maximum likelihood estimation to the Poisson data generated from the MCNPX simulations [8]. These 64 true $f(t)$'s, with 1.0 subtracted, were then inserted into a matrix, A. The SVD of A was calculated, factoring A into three separate matrices:

$$A_{64\times162} = U_{64\times64} S_{64\times64} V^T_{64\times162}, \tag{7}$$

where U is a unitary matrix and S is a diagonal matrix. The basis vectors $B_i(t)$ to be used in this analysis form the columns of V. The significance of this mathematical representation of A is that any one of the $f(t)$'s contained in matrix A^T can be represented by a linear combination of the basis vectors $B_i(t)$. Furthermore, the diagonal matrix S contains the singular values of A. The greater the singular value, the more closely the corresponding vector in V approximates the $f(t)$'s in A^T. From the analysis, it was determined that the five basis vectors with the largest singular values adequately describe the $f(t)$'s; increasing the number of basis vectors did not significantly improve the results. The $f(t)$'s were thus approximated mathematically by

$$f(t) \approx 1.0 + \sum_{j=1}^{5} b_j B_j(t), \tag{8}$$

where b_j are constants. Then, the decomposition of $f(t)$ given by (8) was substituted into (4) with the m_i's left as unknowns. A nonlinear maximum likelihood estimation to the Poisson data generated from the MCNPX simulations was used to solve for the m_i's [8].

The algorithm has a practical limitation as currently implemented. All 64 fuel assembly models were used as a calibration set to determine the empirical $B_j(t)$'s in (8). Conducting 64 calibration measurements, to form the basis set is impractical. Efforts are underway to evaluate the use of smaller subsets of the 64 fuel assemblies to generate the $B_j(t)$'s and to understand how those smaller subsets may impact the uncertainties.

3.1.3 Results for PNNL Empirical Approach

Results using the empirical approach are shown in Figure 3-3. The figure compares the masses for ^{235}U, ^{239}Pu, and ^{241}Pu as estimated from the algorithm versus the true masses for each of the LANL 64 used fuel assemblies. Previous results had been shown recently in [10]. Those results were based on throwing 10^7 source neutrons; note that variation reduction techniques enable a significant reduction of thrown neutrons in the simulation compared to physical neutrons. More recent results shown in Figure 3-3 were generated with four times as many source neutrons as in [10]. The average percent error, $\langle\varepsilon\rangle$, as well as the maximum percent error, ε_m, over each set of 16 fuels having the same level of burnup, is also shown. For Pu, $\langle\varepsilon\rangle$ and ε_m are given for the sum of ^{239}Pu and ^{241}Pu. The results show significant improvement over previous results using the analytical model [8].

A side-by-side comparison among the results shown in Figure 3-3, the results obtained using the same empirical algorithm but with fewer source neutrons [10], and the first generation analytical algorithm with 5 isotopes [8], and the analytical model with 11 isotopes [10] is presented in Table 1. From this table, one can see that the increase in the number of thrown neutrons significantly reduces the both the average percent error and maximum percent error. This result suggests that some of the difference between modeled fuel isotopic masses and extracted isotopic masses was due in part to poor statistics in the simulation. In addition, it is clear that the empirical approach, even with the poorer statistics, provide better results the current analytical approach. In addition, with the exception of the ^{235}U mass for 60 GWd/MTU, all of the higher statistical results for the empirical model have average percent errors less than 1.5%.

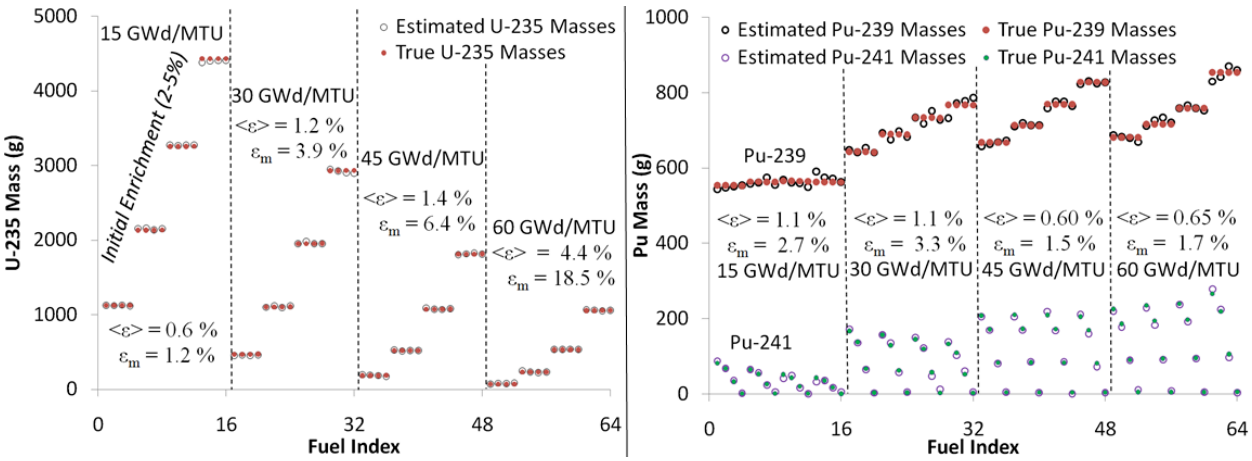

Figure 3-3. LSDS assay results for the LANL 64 used PWR fuel assemblies compared with the true masses read from the MCNPX input decks. Left: ^{235}U; Right: ^{239}Pu and ^{241}Pu. The estimates are represented by open circles; whereas, the true values are represented by closed circles.

Table 1. Average percent error <ε> and maximum percent error ε_m grouped by burnup for the results presented for the empirical algorithm using $4 \cdot 10^7$ source neutrons (Figure 3-3), the empirical algorithm with 10^7 source neutrons [10], and the analytical model with 10^7 source neutrons and 5 isotopes [8], and the analytical model with 10^7 source neutrons and 11 isotopes [10].

Isotope	Method	15 GWd/MTU <ε> | ε_m (%)	30 GWd/MTU <ε> | ε_m (%)	45 GWd/MTU <ε> | ε_m (%)	60 GWd/MTU <ε> | ε_m (%)
^{235}U	Empirical ($4 \cdot 10^7$)	0.6 | 1.2	1.2 | 3.9	1.4 | 6.4	4.4 | 18.5
	Empirical (10^7)	3.3 | 11	3.7 | 16	4.3 | 8.7	6.7 | 22
	Analytical (5 iso)	11 | 19	13 | 31	39 | 120	125 | 390
	Analytical (11 iso)	9.2 | 19	12 | 37	31 | 88	82 | 230
^{239}Pu + ^{241}Pu	Empirical ($4 \cdot 10^7$)	1.1 | 2.7	1.1 | 3.3	0.60 | 1.5	0.65 | 1.7
	Empirical (10^7)	2.8 | 7.5	2.4 | 7.7	3.8 | 11	5.8 | 21
	Analytical (5 iso)	4.0 | 11	4.4 | 12	4.4 | 11	4.5 | 12
	Analytical (11 iso)	9.1 | 20	6.6 | 14	8.5 | 17	10 | 23

An analysis was performed in order to determine whether running the MCNP simulations with additional particles would improve upon the average errors reported above. In addition, the results of the uncertainty analysis were used to determine the number of neutrons that would be required in practice to achieve the statistical precision on which the calculated mass estimates shown in Figure 3-3 were based. This analysis is discussed below.

Results illustrating the average percent error for the ^{235}U and ^{239}Pu mass estimates versus average number of counts tallied in the ^{238}U assay fission chamber detectors are shown in Figure 3-4. The neutron slowing-down times were limited to between 20 μs and 2000 μs. The average percent errors for the ^{235}U mass estimates were much larger for the cases where fewer counts were detected in the assay chambers. In contrast, the average percent errors for the ^{239}Pu mass estimates were relatively insensitive to the average number of tallied counts in the assay detectors.

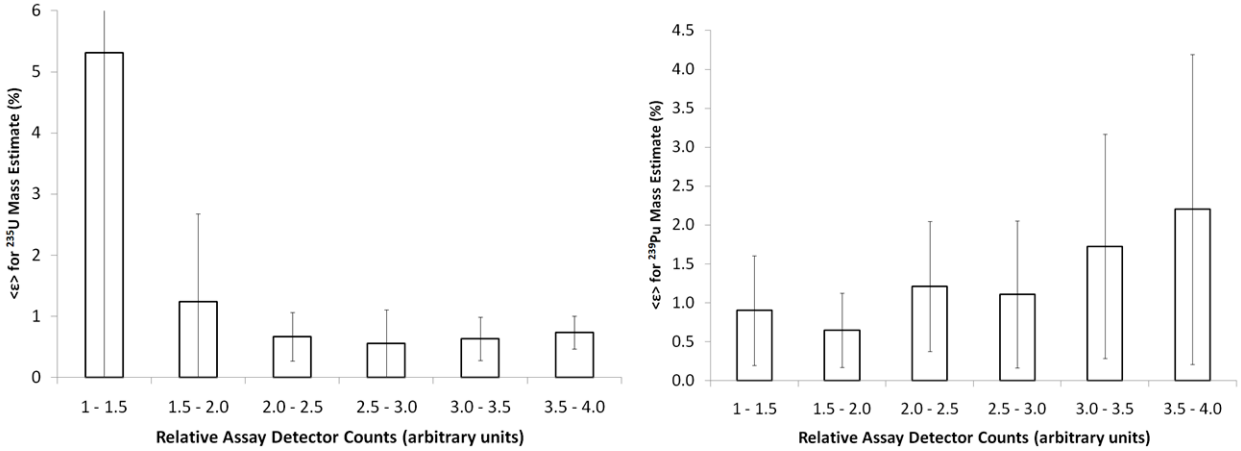

Figure 3-4. Calculated mass percent error, <ε>, averaged over fuel assemblies within bins having the specified number of relative assay detector counts between neutron slowing-down times of 20 μs and 2000 μs for ^{235}U (left image) and ^{239}Pu (right image). The error bars correspond to the standard deviation of the average error among assemblies within each bin of assay detector counts.

Additional analysis was performed comparing the percent error for the calculated mass estimates versus the total mass of the respective isotope present in the used fuel assembly. The results of this analysis are shown in Figure 3-5 for ^{235}U, ^{239}Pu, ^{241}Pu, and all three fissile isotopes together. The largest percent errors for ^{235}U were obtained for the fuel assemblies containing the lowest total mass of ^{235}U present in the entire fuel assembly. For three out of the four assemblies containing less than 100 g of ^{235}U, the calculated ^{235}U mass differed from the true mass by more than 10 %. The percent error for the ^{239}Pu calculated estimates was fairly insensitive to the total mass of ^{239}Pu in the fuel assembly. This may be a consequence of all of the fuel assemblies containing ^{239}Pu masses greater than 500 g and of smaller variations in the mass of ^{239}Pu across the LANL 64 used fuel assemblies. For ^{241}Pu, significantly larger percent errors were obtained for the calculated mass estimates, particularly for masses less than 10 g. Therefore, it was concluded that additional MCNP simulations with greater numbers of source neutrons would be unnecessary, as the accuracy of the calculated mass estimates appears to be limited by the total amount of the respective isotope present in the used fuel assembly. In addition, these results suggest that the inspection of some assemblies may benefit from longer measurement times.

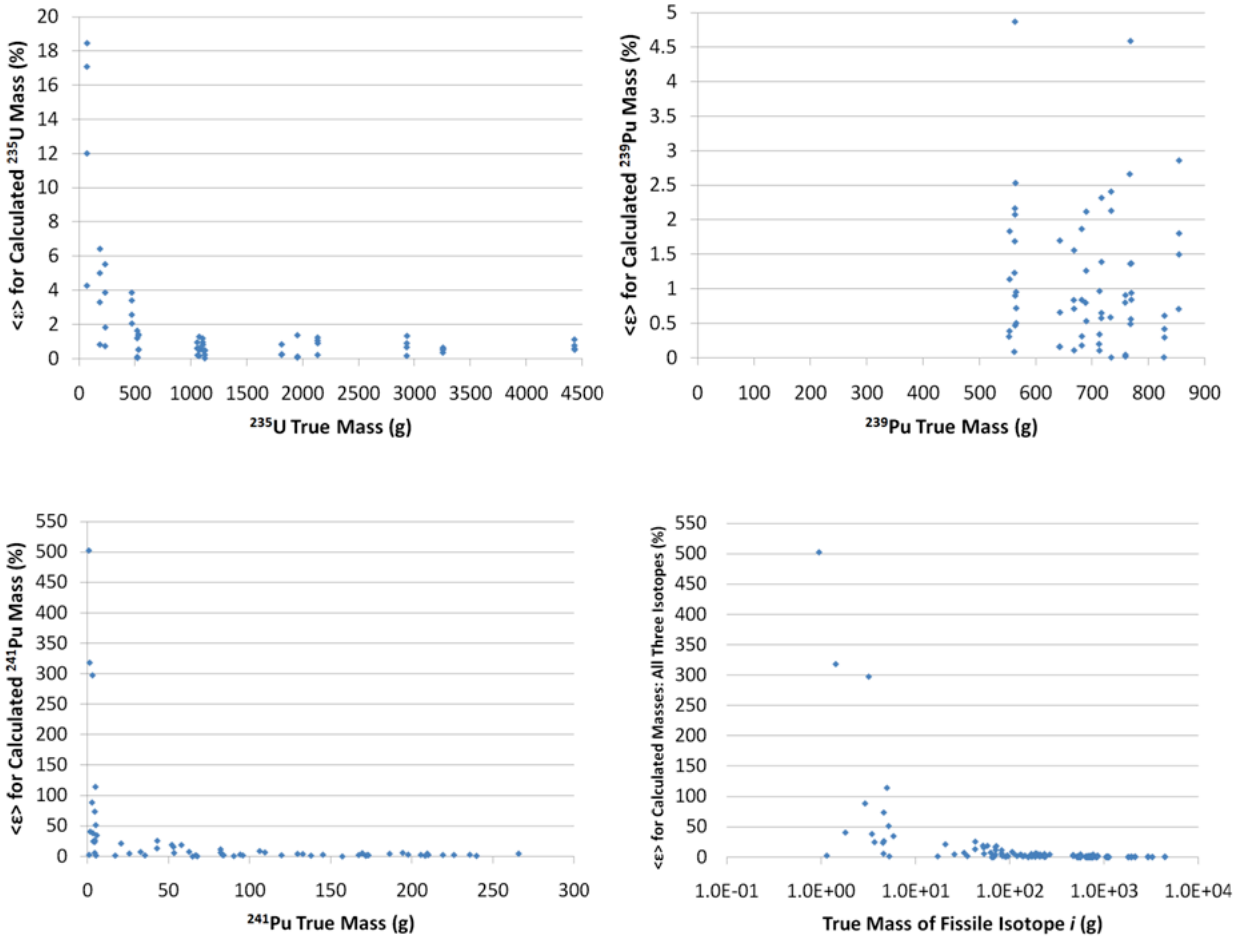

Figure 3-5. Calculated mass percent error, <ε>, versus the total true mass of the respective isotope in the used fuel assembly.

In addition, three of the 64 fuels were simulated without variance reduction (VR). In the 20 μs to 2000 μs neutron slowing-down region, the fractional errors associated with the tallied counts in the ^{238}U assay detector for these three simulations were then compared to fractional errors for the MCNP simulations using VR for the same three fuels. From this comparison, the total number of source neutrons required, without using VR, to achieve the same level of statistical precision as that without using VR, across all time bins in the slowing-down region of interest, was determined. To determine the total number of source neutrons required in an actual LSDS of the same design that was modeled in the simulations, the calculated result for the total number of source neutrons required without using VR was multiplied by an assumed absolute detection efficiency of 0.1% for the 32 ^{238}U assay detectors combined, as estimated in a previous report [8]. The results of this calculation are given in Table 2. From these preliminary results, the original assumption in [8] of a total of 10^{16} source neutrons required for an assay of a used fuel

assembly seems reasonable, and is similar to the LANL conclusions discussed below. Such an assay can theoretically be completed comfortably within an hour with the use of a LINAC as a pulsed neutron source.

Table 2. Number of source neutrons required in an experiment to achieve the same statistical precision across all time bins in the ^{238}U assay signal as the results upon which the calculated mass estimates presented in this report were based.

Fuel Index (#)	Burnup (GWd/MTU)	Initial Enrichment (%)	Cooling Time (yr)	MCNP Source Neutrons (Using VR)	MCNP Scaled Source Neutrons (No VR)	Actual LSDS Required Source Neutrons
23	30	3	20	$4\cdot10^{7}$	$1.4\cdot10^{12}$	$1.4\cdot10^{15}$
36	45	2	80		$1.6\cdot10^{12}$	$1.6\cdot10^{15}$
52	60	2	80		$1.9\cdot10^{12}$	$1.9\cdot10^{15}$

3.2 LANL Analytical Method

Analysis of LSDS spectra requires the identification of the major fissile isotopes, the major neutron absorbers, and the hydrogen content in the PWR fuel assembly. In order to analyze the results, one runs a simulation code (MCNPX) varying the input parameters as needed to converge on the experimental results. A quicker but less precise approach is to use the analytical model presented in [11] including the modifications described in [12]. The model accounts for attenuation of a neutron beam due to fission and absorption in the fuel, effects of hydrogen, absorption by fission products and simplified cylinders for fuel. This model allows one to quickly obtain approximate results (e.g., from MCNPX), by adjusting the input values that are required to fit the data.

The same model can be used as a tool to estimate the errors inherent in analysis process. Given an analytical model-generated spectrum, one can vary the concentrations of the fissile isotopes and calculate the variation between the starting spectrum and the changed spectrum using a χ^2 metric. Specifically, if N_i is the number of counts in channel i of the LSDS spectrum for specific concentrations of ^{235}U, ^{239}Pu and ^{241}Pu, changing these values results in a new spectrum with N_i' counts in channel i. χ^2 is then given by

$$\chi^2 = \sum_{i=1}^{M} \left(N_i - N_i' \right) / \sigma_i^2 , \qquad (9)$$

where σ_i is approximately given by $\sqrt{N_i}$, and M is the total number of channels.

In the original study [11], variations in the different Pu isotopes provided orthogonal changes in χ^2. This implied that measurement uncertainties of one isotope would not impact those of another isotope. In the current analysis, which uses a more detailed used fuel inventory, the uncertainties of one isotope do impact the uncertainties of another isotope, i.e. the measurements of these isotopes are correlated. This is demonstrated in Figure 3-6 which shows that the changes in χ^2 per degree of freedom as a function of the relative deviation from the correct values of ^{239}Pu and ^{241}Pu. The initial ^{239}Pu mass fraction is 0.5%, and the ^{241}Pu fraction is 0.22 times the ^{239}Pu mass. This ratio is for 45 GWD/MTU PWR fuel burnup, and we assume 10^{16} interrogating neutrons in the LSDS. Figure 3-7 shows details extracted from Figure 3-6 – for relative errors of 0, -2% and -4% in the ^{241}Pu concentration, the minimum of the χ^2 shifts the concentration of ^{239}Pu, from 0% to + 0.75% to +1.5%.

The contour plot demonstrates that if the mass of ^{241}Pu is wrong by 2% (in either direction) ^{241}Pu, then the minimum in χ^2 will change by approximately 1% in ^{239}Pu. The conclusion is that within this model it is extremely important to find the correct absolute minimum of χ^2. Likewise, any systematic errors in the analysis of experimental LSDS time spectrum, either by MCNPX simulation or an analytical model, need to be minimized in order to obtain an unbiased result.

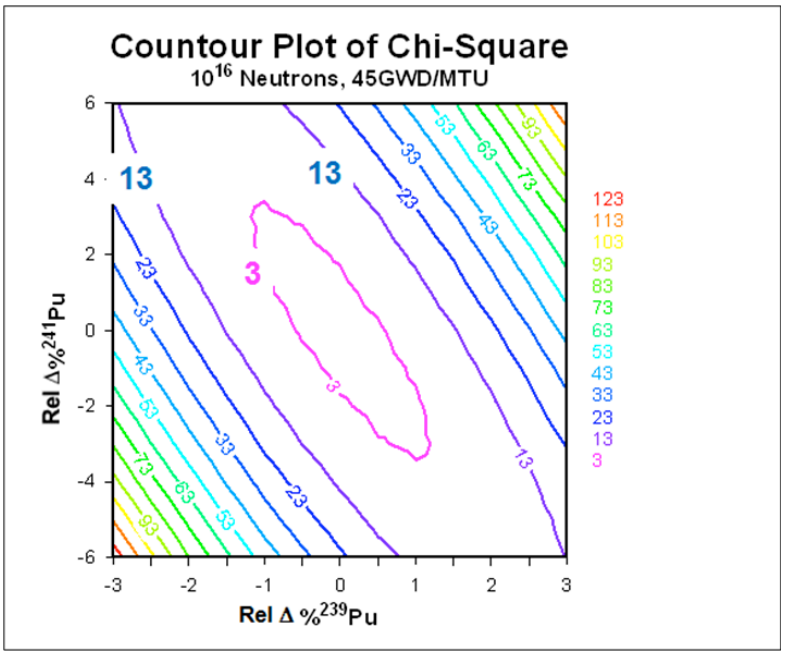

Figure 3-6. χ^2 contour plot, as a function of the relative change in ^{239}Pu and ^{241}Pu from the input values to the analytical model.

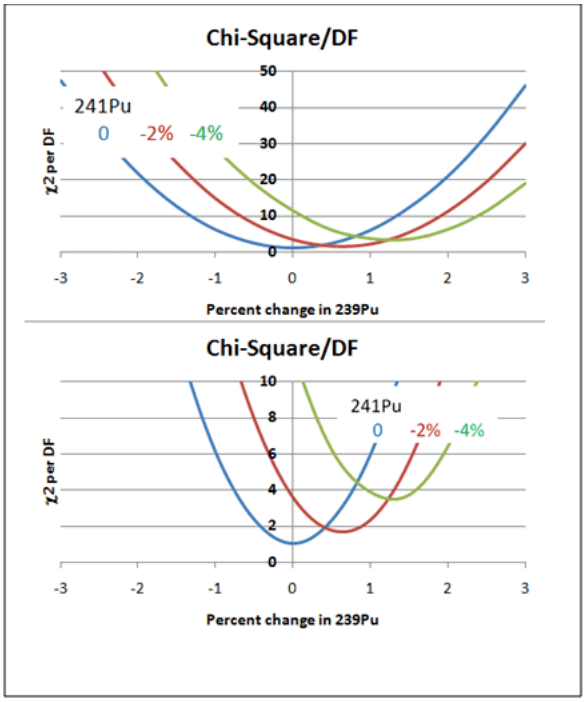

Figure 3-7. Projections of the χ^2 contour plot, that show the change in the location of the minimum for different values of ^{241}Pu.

Impact of systematic errors

From these last two plots based on the LANL model, the concentration of ^{239}Pu could be determined to a precision of 1% or better using an interrogating neutron source totaling 10^{16} neutrons in the absence of systematic errors. Systematic errors could limit the accuracy by keeping χ^2 at a higher minimal value. For example, if systematic errors were to prevent it from going below 20 (this number is totally arbitrary), Figure 3-8 shows the estimated uncertainties in the concentrations of the various fissile materials and hydrogen. The hydrogen concentration in the zircalloy fuel cladding was assumed to be 10 ppm per GWD/MTU. In this case, the LSDS analysis would determine its concentration with a precision of a few percent. This may be useful for confirming the history of fuel bundles, in addition to the information provided by the fissile isotopes. Note that the ^{240}Pu concentration is determined in this process, although with a significantly lower precision. This is due to the impact of its *absorption* resonance on the spectrum, since it has no fission resonance (it is a threshold fissioning isotope).

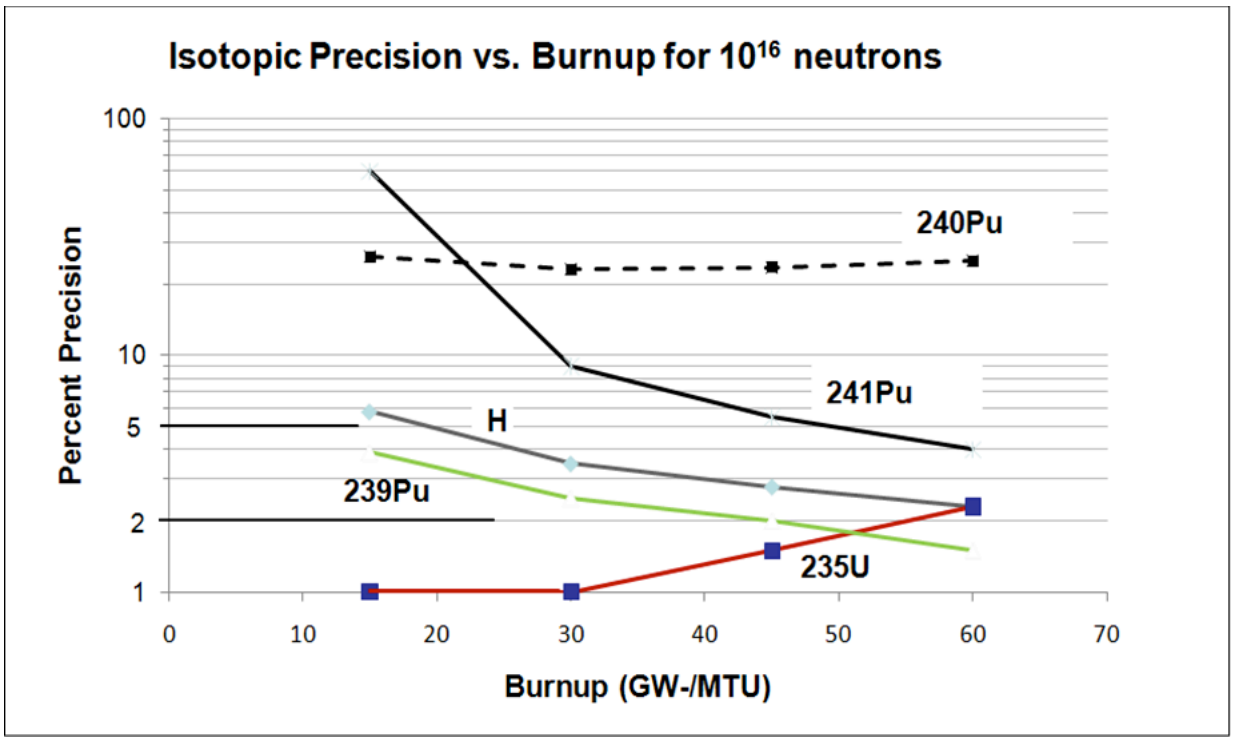

Figure 3-8. Systematic errors in isotope concentrations assuming that the minimum value of χ^2 is 20 due to systematic errors.

3.3 TIME SPECTRAL ANALYSIS CONCLUSIONS

The potential for the LSDS to provide direct, independent, and accurate assay of U and Pu isotopes in used fuel relies heavily on developing time-spectra analysis methods that can account for the nonlinear effects of self-shielding and neutron absorption by non-fissile isotopes. The time-spectra analysis method development efforts from FY2011 were evaluated using a (LANL-developed) simulated library of PWR used fuel assemblies that spans a wide range of initial enrichment, burnup, cooling time (and included pin-to-pin and within-pin burnup variation). The major conclusions of the FY2011 evaluation of the time spectral analysis algorithm are summarized below:

For the wide parameter space spanned by the LANL 64 used fuel assemblies, the calibration-based SVD algorithm allows the direct and independent assay of ^{239}Pu and ^{241}Pu to an accuracy within approximately 3%. Using all 64 LANL fuels in the calibration to generate five empirical basis vectors, the accuracy for the sum of the masses of ^{239}Pu and ^{241}Pu was determined within 3.3% for each of the LANL 64 fuel assemblies. For 90% of the assemblies, this sum was calculated to within 2% accuracy, and for 65% of the assemblies, the accuracy was determined to within 1%. The accuracy of this calibration method now appears to be limited by the overall

sensitivity of the LSDS in detecting small total amounts of fissile isotopes present in the fuel assemblies. Similar results are obtained using the LANL perturbation approach.

Significant changes to the first generation analytical model are necessary in order to account for the scattering and streaming within the fuel assembly. Insertion of the cross-sections of additional absorbers into Eq. (6) presented little benefit and investigation of the neutron paths across the assemblies demonstrated the necessity to develop a new analytical form for $f(t)$.

3.4 TIME SPECTRAL ANALYSIS FUTURE WORK

Further study is needed to test and develop confidence in the calibration-based algorithm. Therefore, the algorithm will be tested with a subset of the LANL 64 used fuel assemblies to generate the calibration data for numerically estimating the time-dependent self-shielding functions. In addition, the algorithm will be tested on models of fuels having different initial enrichments, burnups and/or cooling times than those of the LANL 64 used fuel assemblies.

The first generation analytical model will be modified in an attempt to accurately account for the streaming, scattering, and absorption that is occurring within the fuel assemblies and is not appropriately accounted for at present. This modification will proceed by a close inspection of the neutron physics occurring due to simplified interrogation targets, such as single pins and pin arrays representing sections of assemblies. This procedure will provide insight into the quantification of the importance of streaming, scattering and absorption in the fuel assemblies. A new semi-empirical model will be generated from these studies that will in turn be used to gain insight into the generation of a new fully analytical model.

The incorporation of additional information will be investigated. These may include estimates of burnup from measurements using $^{134}Cs/^{137}Cs$ gamma-ray peak ratios or limited operator-provided information, which if incorrect, would cause the results to significantly diverge. Such information can be incorporated into the calibration algorithm by enabling one to bias the selection of fuels used in the calibration set.

Future efforts must also include the benchmarking of the calibration algorithm with the experimental data from actual LSDS instruments, such as those available at the LANL LANSCE facility and the Gaerttner LINAC facility at RPI. For example, the calibration algorithm can be applied to the RPI fresh fuel pin measurements by using MCNP to generate calibration data by simulating the assay of a single fuel pin and varying its isotopic fuel composition.

4.0 Threshold Neutron Sensor Development

Efficient fast neutron detection is the key instrumentation challenge for successful development of the LSDS approach. The ISU and UNLV collaborative effort is focused on the fabrication and testing of prototype fission chambers lined with ultra-depleted ^{238}U and ^{232}Th. The testing of

fission chambers (FC's) for characterization purposes is currently being done in the LSDS instruments at LANL and at RPI.

ISU has in its possession NIST quality deposits of ^{235}U, ^{238}U, ^{239}Pu, ^{237}Np, and ^{240}Pu to be used in special back-to-back (BTB) FC's. Shown in the left pane of Figure 4-1 is a 1.8 cm diameter deposit of ^{237}Np and a BTB FC, which measures a little over 4 inches in length. UNLV has been successful at U deposition on a stainless steel disc (SS) using spiked U_3O_8 from Room Temperature Ionic Liquid (RTIL). The right pane of Figure 4-1 shows this deposition of U on a SS disc. A second deposition was improved, with respect to the thickness, and continued progress is expected.

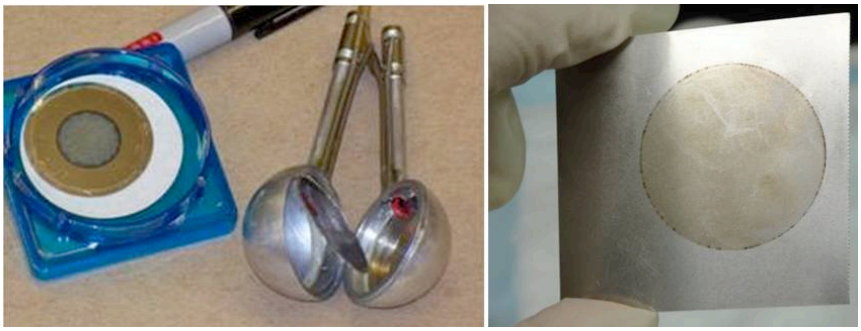

Figure 4-1. Left Pane: On the far left is a foil containing a 1.8 cm diameter deposit of ^{237}Np, and on the right is an open back-to-back (BTB) fission chamber (FC), consisting of two 2-π ionization detectors, showing the metallic tray which will be used to support both the ^{237}Np-coated foil and a foil coated with uDu. Right Pane: First successful deposition of U, using spiked U_3O_8 from RTIL, on a SS disc for use in BTB FC's.

Figure 4-2. shows the LANL ^{232}Th chamber (left upper) and preamp combination that was used for FY11 run cycle experiments. The chamber contains a total of 37 milligrams of ^{232}Th, and is "compensated" – the signals with and wthout the ^{232}Th foils are subtracted to reduce the background produced by the initial high-intensity pulse in the chamber. Analysis of the spectrum we obtained with it shows that there is roughly a 4 ppm contamination of ^{235}U. However, the background produced by this contamination is easily subtracted.

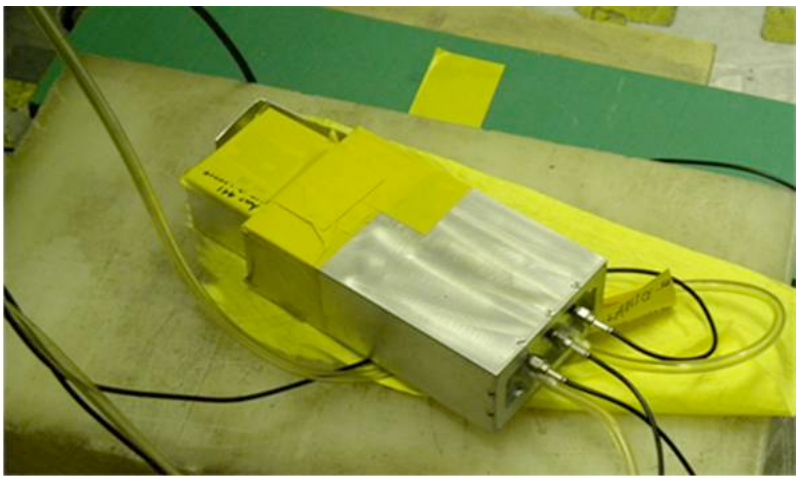

Figure 4-2. The LANL ^{232}Th chamber and preamp combination that was used for FY2011 run cycle experiments.

5.0 Benchmarking

In addition to theoretical modeling and simulation, empirical benchmarking is being conducted with available LSDS instruments at LANL and RPI in order to ensure that the physical phenomena are modeled and simulated correctly and to verify the accuracy of the nuclear cross section data used in the models and MCNP simulations. Experiments conducted at these facilities are also being used in order to characterize the detectors being developed by LANL, ISU and UNLV.

5.1 LANL Benchmarking

The neutron source for the LSDS at the Los Alamos Neutron Science Center (LANSCE) is generated by impinging protons from the 800 MeV LINAC onto a tungsten target. Measurements were conducted with 23 gram sample of ^{235}U and a threshold neutron detector made of 37.5 mg of ^{232}Th foils placed in the LSDS at the LANSCE facility. Measurements were conducted both with and without the ^{235}U sample. Results from measurements with the sample are shown in Figure 5-1 while those without the sample on shown in Figure 5-2.

It was found that there was a measureable contamination of ^{235}U in the ^{232}Th foils. If the ^{232}Th in the threshold detector was pure, no counts should have been observed in the background run (without the ^{235}U sample). However, a significant number of counts were observed in the background run which could be explained by a ^{235}U contamination of the ^{232}Th at a level of 5 ppm. This contribution was then subtracted from the time spectrum when the ^{235}U sample was introduced, to obtain the spectrum due to the interaction of high-energy neutrons with the ^{232}Th

in the detector. Although unexpected, there is an advantage to having this contamination: it provides an independent measurement of the flux as a function of time, using ^{235}U which is a well-measured standard.

The width of the peaks in the spectra indicated a measureable hydrogen content in the lead. The widths peaks in the measured spectra were broader than those in the simulation. Adding 2 ppm hydrogen to the lead considerably improved the fit. This level of hydrogen content is comparable to the hydrogen content found elsewhere in pure lead.

As seen in Figures 5-1 and 5-2**Error! Reference source not found.**, generally good agreement exists between the MCNP calculations and the experimental data. However, it is noted that MCNP-calculated results, represented by the black lines, fall below the experimental data, particularly above 200 μs. It is believed that the source of this discrepancy may be attributed to the nuclear data, as a large difference in neutron flux at long slowing-down times exists when using the ENDF-B/VI as compared to the ENDF-B/VII neutron libraries.

Further efforts by LANL will include the use of a Pu sample, which is expected to provide more counts at longer-slowing down times (e.g. $t > 500\mu s$), to help identify the source of the discrepancy between the experimental data and MCNPX simulation shown in **Error! Reference source not found.**, and demonstrate the ability to fit and quantify a source with Pu content. Further LANL efforts may also include testing a helium-filled proportional counter, and the consideration of a perturbation model to analyze LSDS used fuel spectra.

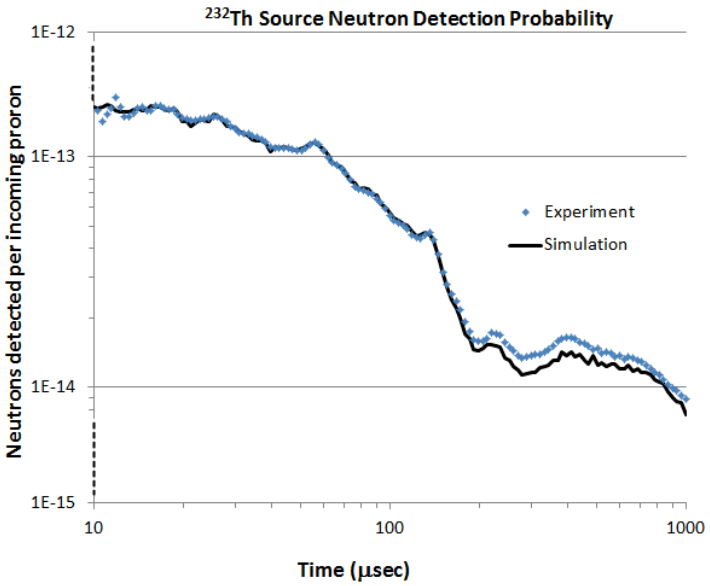

Figure 5-1. Experimental data compared to MCNPX simulation results of the signal from a fission neutron detector consisting of 37.5 mg of ^{232}Th foils for which a fission neutron source consisting of 23 grams of ^{235}U was placed in the LSDS at the LANSCE facility.

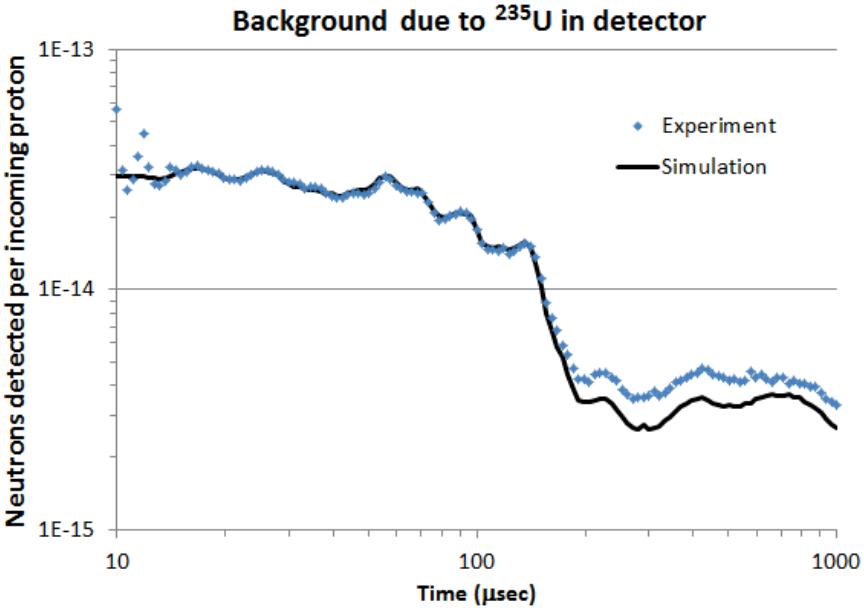

Figure 5-2. Same as Figure 5-1, but with the ^{235}U source removed from the LSDS. Spectrum is due to ^{235}U deposit in the thorium detectors. Note the difference in vertical scale with Figure 5-1.

5.2 RPI Benchmarking

Experimental results have also been generated by RPI using its LSDS instrument at the Gaerttner Linear Accelerator (LINAC) Laboratory in which neutrons are generated by impinging the 58 MeV electron beam from the LINAC onto a tantalum target. Shown in Figure 5-3 is a ^{238}U assay detector response for a fresh fuel pin assay, in which a fresh fuel pin containing 32.5 g of ^{235}U was placed inside the LSDS. Also shown in the figure are MCNP simulation results assuming various concentrations of hydrogen content in the Pb. The MCNP simulations for 2 ppm of hydrogen content in the Pb of the LSDS yields very good agreement with the experimental data, suggesting the presence of 2 ppm of hydrogen content in the RPI LSDS lead. Differences between the measurement and simulation at shorter slowing down times are attributed to inaccuracies in the ^{238}U cross section for the subthreshold fission reaction.

It is worthwhile comparing the Figure 5-2, measurement of U-235 sample by LANL and Figure 5-3, measurement of a fresh fuel pin at RPI. Both figures show strongest differences between experimental data and simulation results above 200 μs. In the case of the RPI results, the difference is attributed to hydrogen content of the lead, which nicely brings the experimental data and simulation results into agreement. The LANL analysis determined the hydrogen content of their lead by fitting the widths of the peaks. Further analysis is required to understand the comparison of the modeling results with the experimental data shown in the two figures.

Experimental results for two additional experiments are shown in Figure 5-4. The plot on the left illustrates the assay detector response in which a PuBe source containing 96 grams of ^{239}Pu was placed inside the RPI LSDS. As shown, the agreement between the simulation and measurement is very good. From this experiment, the assay detector was found to be essentially insensitive to the constant gamma background of the PuBe source, and the constant neutron background of the PuBe source was easily overcome by the significantly higher number of fission neutrons induced by the interrogation neutron flux from the LINAC. Experimental data (open shapes) and MCNP simulation results (solid lines) are shown in the right-hand plot of Figure 5-4, for which both the fuel pin and PuBe source were placed inside the RPI LSDS, and the PuBe source was placed at various distances from the assay detectors to simulate various amounts of ^{239}Pu. As shown, the detector response clearly exhibits characteristics of both the ^{239}Pu and ^{235}U.

In order to evaluate the assay sensitivity for ^{235}U, measurements of a fresh fuel pin combined with additional small amounts of ^{235}U were conducted. Assays with 1, 3, 5 and 10 discs, each consisting of 0.2 – 0.3 g of ^{235}U, were performed. Two different flux monitors were used to take into account accelerator dependent changes in the LSDS flux level when comparing different assays. The left side of Figure 5-5 shows the response of a ^{238}U assay detector for an assay of a fuel pin and of a fuel pin with 10 ^{235}U discs of a total amount of 2.6308 g additional ^{235}U. The increase of the count rate due to the additional fissile material is clearly shown. The right side of Figure 5-5 shows the increase of the detector count rate when discs are added to the fuel pin in

the assay based on an integrated count rate in the time frame from 30 to 110 μs. The data were corrected for detector background signal caused by the interrogation neutron flux interacting directly with the assay detector. Experimental results (symbols) and MCNP simulation results (solid line) are shown. The adding of a single disc with about 260 mg of ^{235}U can be distinguished from the fuel pin assay. Note that due to geometric effects the assay detector sees effectively about 10 g of ^{235}U from the fuel pin.

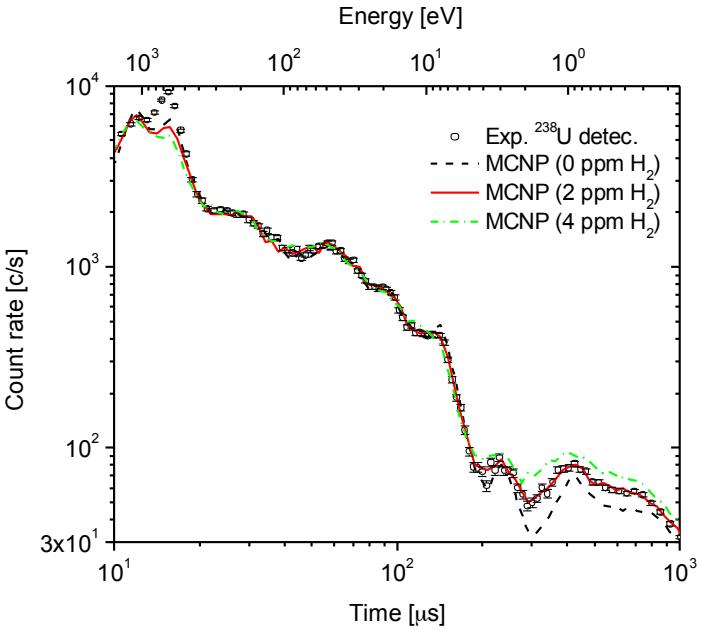

Figure 5-3. A ^{238}U assay detector response for a fresh fuel pin assay, in which a fresh fuel pin containing 32.5 g of ^{235}U was placed inside the LSDS at RPI, compared with MCNP simulation results assuming various concentrations of hydrogen content in the Pb.

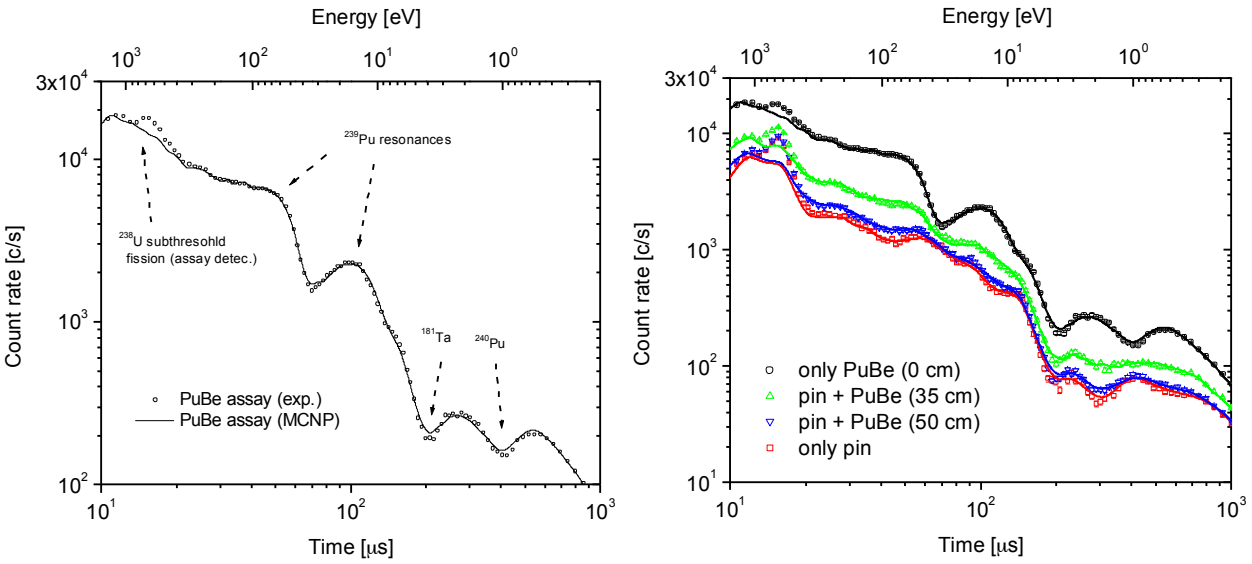

Figure 5-4. LEFT: Experimental data (open shapes) and MCNP simulation results (solid lines) for the assay detector response in which a PuBe source containing 96 grams of ^{239}Pu was placed inside the RPI LSDS. RIGHT: Experimental data and MCNP simulation results (solid lines) for the assay detector response in which both the PuBe source (at various distances from the detector) and fresh fuel pin were placed inside the RPI LSDS.

A combined assay of a fuel pin, the PuBe source (at 30 cm distance from the detector) and 1 or 3 ^{235}U discs was performed. Figure 5-6 shows a comparison of the assay detector count rate with and without 3 added discs. In comparison to an assay of a fuel pin and the PuBe source these cases are planned to be used to test deconvoluting algorithms in the linear approximation which is currently being investigated. A preliminary deconvolution based on the 30 - 670 μs time frame indicates an increase of the ^{235}U contribution by about 7% as well as an increase of the PuBe contribution by about 2.4 %. The increase of the ^{235}U contribution is in agreement with the results of Figure 5-6 while the increase of the PuBe should be zero and might be explained by a slight displacement of the PuBe source. Further work including full simulations is in progress.

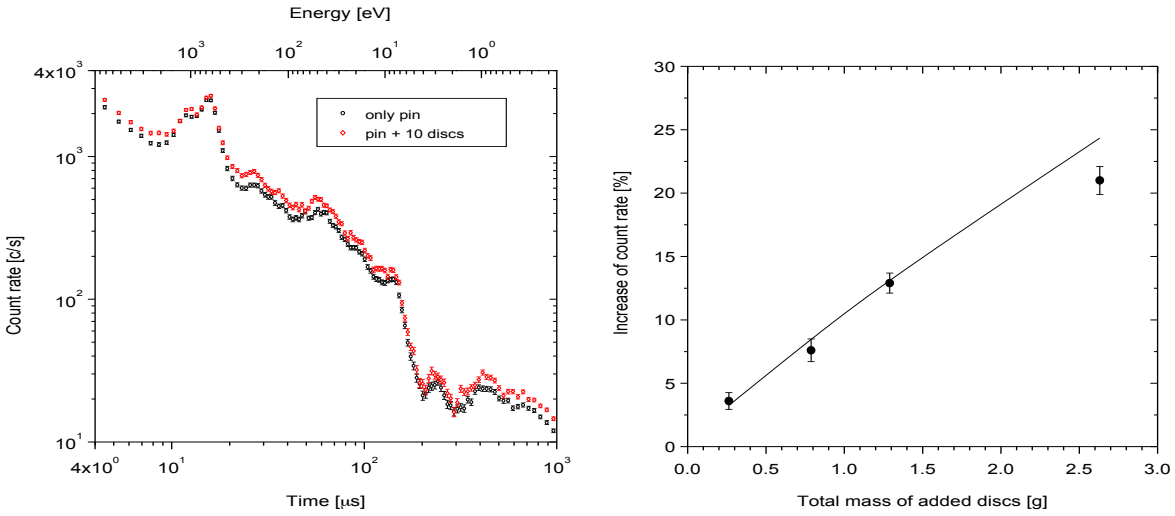

Figure 5-5. LEFT: Experimental data for the assay detector response in which a fuel pin and a fuel pin plus 10 ^{235}U discs were placed inside the RPI LSDS. RIGHT: Experimental data and MCNP simulation result (solid line) for the increase of the detector count rate when ^{235}U discs are added to the fuel pin assay

Future efforts at RPI will include the assay of an entire fuel assembly for the study of self-shielding effects as well as the ability to detect diversion by detecting a missing fuel pin in the fuel assembly.

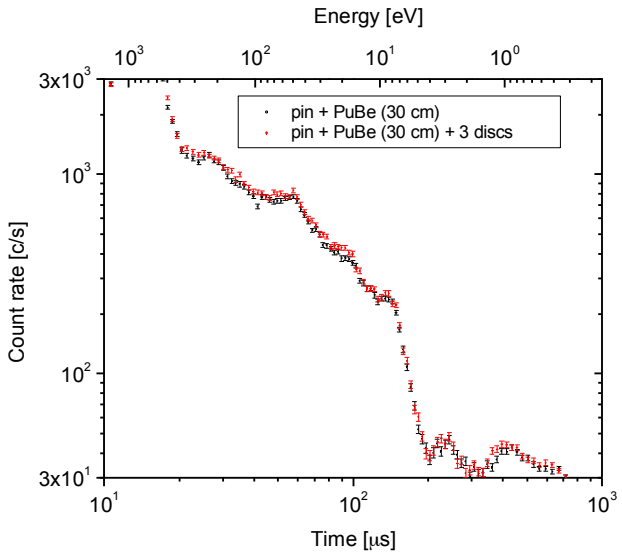

Figure 5-6. Comparison of the detector count rate of an assay of a fuel pin + PuBe source and of a fuel pin + PuBe source + 3 ^{235}U discs

6.0 Summary and Future Work

Efforts in FY2011 on time spectral analysis algorithms, threshold neutron sensor development, and empirical benchmarking and modeling and simulation have confirmed the potential of LSDS for direct, independent assay of U and Pu isotopes in used fuel. PNNL has developed an empirical approach for determining the self-attenuation function that determines the isotopic masses to below 3%. Benchmarking of simulations and measurements performed by LANL and RPI show good agreement over much of the time domain. In addition measurements have shown sensitivity to small quantities of ^{235}U. Progress is being made on developing threshold fission chambers by UNLV and ISU.

In FY2012, PNNL will continue to develop the empirical model. The model will be tested on a subset of the LANL used fuel assembly library to generate calibrations to determine the impact of a smaller calibration data set. The empirical algorithm will be evaluated on used fuels having different initial enrichments, burnups, and cooling times than those spanned by the LANL used fuel library as additional tests. Some effort will be directed to continuing to understand and refine the analytical approach. Algorithm efforts will continue to focus on realizing LSDS as an independent, direct NDA measurement approach for fuel assay. However, other approaches that incorporate additional information will be considered and explored including estimates of burnup from measurements using ^{134}Cs / ^{137}Cs gamma-ray peak ratios, limited operator-provided information, which if incorrect, causes the results to significantly diverge. In addition, the concept of using algorithms that rely less on calibration data will continue to be investigated.

In FY2012, the development of threshold neutron detectors will continue, and UNLV will calibrate existing uDU deposits at ISU. Future work also includes the production of new uDU foils using a unique approach for metal deposition on gold substrates. ^{232}Th will be acquired, and calibrated deposits will be used for back-to-back fission chambers. The design of large ^{232}Th fission chambers for LSDS testing will be considered in comparison to helium-filled proportional counters that will be tested at LANL. Fission chambers will continue to be tested at LANSCE and RPI.

Additional measurements are planned at LANSCE and RPI. Further efforts by LANL will include the use of a Pu sample, which is expected to provide more counts at longer-slowing down times (e.g. $t > 500\mu s$), to help identify the source of the discrepancy between the experimental data and MCNPX simulation, and demonstrate the ability to fit and quantify a source with Pu content. Further efforts may also include the consideration of a perturbation model to analyze LSDS used fuel spectra. Future efforts at RPI will include the assay of an entire fuel assembly for the study of self-shielding effects as well as the ability to detect diversion by detecting a missing fuel pin in the fuel assembly.

7.0 References

1. N. Peter, "A Shipper-Receiver-Difference Approach for Reprocessing Plants," 8th International Conference on Facility Operations – Safeguards Interface, Portland OR, 2008.

2. Y. Danon, et al, "Measurements with the high flux lead slowing-down spectrometer at LANL," *Nuclear Instruments and Methods in Physics Research B*, 261/1-2, pp. 953-955, 2007.

3. C. Romano, et al, "Measurements of (n,α) cross-section of small samples using a lead-slowing-down-spectrometer," *Nuclear Instruments and Methods in Physics Research A*, 562/2, pp. 771-773, 2006.

4. D. B. Pelowitz, "MCNPX User's Manual", Vol. LA-CP-07-1473 Version 2.60, Department of Energy, Los Alamos National Laboratory, Los Alamos, NM: U.S., 2008.

5. Y. D. Lee, et al. "Design of a Spent-Fuel Assay Device Using a Lead Spectrometer," *Nucl. Sci. Eng.* 131/1, pp. 45-61, 1999.

6. L.E. Smith, K.K. Anderson, J.J. Ressler, S.D. Kiff, M.W. Shaver, "Time-Spectral Analysis Algorithms for Lead Slowing-Down Spectroscopy of Spent Fuel," 2010 INMM Annual Meeting, Baltimore, MD (2010).

7. S.J. Tobin, et al., "Determination of Plutonium Content in Spent Fuel with Nondestructive Assay," 2009 Institute of Nuclear Materials Management Conference, Tucson, AZ, 2009.

8. L. E. Smith, C. J. Gesh, K. K. Anderson, A. M. Casella, and M. W. Shaver, "Lead Slowing-Down Spectroscopy for Direct Measurement of Plutonium in Spent Fuel: NGSI Phase I Report. PNNL-20158, Pacific Northwest National Laboratory, Richland, WA. 2010.

9. G. H. Golub and C. Reinsch, "Singular Values and Least Squares Solutions," *Numer. Math.* 14, pp. 403-420, 1970.

10. J. A. Kulisek, et al, "Progress on Establishing the Feasibility of Lead Slowing Down Spectroscopy for Direct Measurement of Plutonium in Used Fuel," 2011 Institute of Nuclear Materials Management Conference, Palm Desert, CA, July 2011.

11. A. Gavron, L. Eric Smith, Jennifer J. Ressler, Nucl. Instr. and Meth. A 602 (2009), 581.

12. A. Gavron, LA-UR-09-06197, Report to the MPACT program on LANL Lead Slowing Down Spectrometer Accomplishments for FY09.

Pacific Northwest
NATIONAL LABORATORY

U.S. DEPARTMENT OF
ENERGY

Proudly Operated by Battelle *Since 1965*

902 Battelle Boulevard
P.O. Box 999
Richland, WA 99352
1-888-375-PNNL (7665)
www.pnl.gov